Journal of Mines, Metals and Fuels, *71(12D) : 190-193; 2023. DOI: 10.18311/jmmf/2023/47998*

Print ISSN : 0022-2755

Journal of Mines, Metals and Fuels

Contents available at: *www.informaticsjournals.com/index.php/jmmf*

Structural and Optical Properties of Red Emitting Y_2O_3: Eu Nanophosphor

Soorya G. Nath[1] and E. I. Anila[1,2*]

[1]*Union Christian College, Aluva – 683102, Kerala, India; anila.ei@christuniversity.in*

[2]*CHRIST (Deemed to be University), Bengaluru – 560029, Karnataka, India*

Abstract

Europium-doped yttrium oxide is an efficient red phosphor which has commercial significance. In this work Y_2O_3: Eu nanophosphor was prepared using wet chemical precipitation method followed by annealing. The results obtained from the sample's X-ray diffraction experiments indicate that the material exhibits a cubic structure, showcasing an average crystallite size of 19nm. The value of micro strain as well as crystallite size was estimated using a Williamson-Hall plot and the positive value of micro strain thus obtained represents lattice elongation. Also, the corrected value of the lattice parameter established using the Nelson-Riley plot is 10.64Å. Ultraviolet (UV)-vis. absorption spectroscopy was employed for bandgap measurements, resulting in a direct bandgap of 6 eV. There was an increase in bandgap energy with respect to bulk (~5.8eV), which may be due to the size. On exciting the sample at 254nm, intense red emissions with a major peak at 611nm were observed which shows the applicability of this material in luminescence applications.

Keywords: *Cubic Yttrium Oxide, Europium, Intense Red Emission*

1.0 Introduction

Rare earth oxides attract research interest due to their stable chemical and thermal properties, especially in the field of luminescent materials. Yttrium Oxide is one such important rare earth sesquioxide which finds a variety of applications[1,2]. Yttria mainly exists in 3 phases *viz*. cubic, monoclinic and hexagonal among which the cubic phase exhibits more thermal stability which is one of the reasons why more research is focussed on this phase[3,4].

Among the various phosphor host materials, yttrium oxide plays a vital role due to the resemblance of the ionic radius of Y^{3+} with other rare earth ions. Yttrium oxide doped with Europium is one of the most promising red phosphors. The material finds a variety of applications in the display industry[1]. Many reported works are investigating the photoluminescence characteristics of Y_2O_3: Eu nanophosphor[4,5]. Yet, the material is significant due to its efficient luminescence capacity, colour purity, stability etc. Eu^{3+} activated yttrium oxide prepared by different synthesis routes shows differences in its properties such as luminescence behaviour, size, morphology etc. The recognition of mineral composition in rocks can be achieved by studying their unique luminescence characteristics. This is where the significance of rare earth-doped yttrium oxide's excellent luminescence properties comes into play, enabling the identification of its presence in rock samples. In our work, highly intense red-emitting Y_2O_3: Eu nanoparticles are synthesised using a simple wet chemical precipitation method followed by annealing. Compared to the previous reports based on this method on the preparation of Y_2O_3: Eu nanophosphor[6–8], our material was prepared at a lower temperature without the addition of any capping

**Author for correspondence*

agents or flux materials. The material is characterised using X-Ray Diffraction (XRD), UV-Vis-NIR absorption spectroscopy and Photoluminescence (PL) experiments. The Chromaticity (CIE) coordinates were estimated using the PL spectrum. The work mainly emphasises the photoluminescence characteristics of the material.

2.0 Experimental

50ml each of 0.125M Yttrium Nitrate Hexahydrate ($Y(NO_3)_3.6H_2O$, Sigma, 99.8%) and 0.008M Europium Nitrate Pentahydrate ($Eu(NO_3)_3.5H_2O$, Sigma, 99.9%) are prepared in distilled water. 0.3125M Urea (NH_2CONH_2, Nice, 99%) is added to this solution and stirred thoroughly. The solution is then transferred to a capped bottle and kept at 90°C for one day in a hot air oven[9]. The precipitate is separated and washed by centrifugation. The white powder is thoroughly ground using mortar and pestle and annealed at 600°C for 2 hours.

XRD (Rigaku-Miniflex) analysis was performed on the sample to determine its structure. UV-Vis-NIR absorption spectroscopy (Shimadzu) was employed for bandgap measurements and Fluoromax-4C (Horiba) was used to record PL spectra to determine the luminescence characteristics.

3.0 Results and Discussion

The results of the XRD analysis are depicted in Figure 1. Figure 1A represents the XRD spectrum for the sample. On analysing the spectrum, the material is identified as cubic Yttria with major reflections from the planes (2 1 1), (2 2 2), (4 0 0), (4 4 0) and (6 2 2). The data agrees with ICDD File Number: 741828. The slight shift in the peaks can be attributed to the doping effect. The crystallite size (D) is computed using Scherrer formula[10] given by:

$$D = \frac{0.9\,\lambda}{\beta cos\theta} \quad (1)$$

where, λ represents the wavelength of the x-ray source, β and θ symbolise the full width at half maximum and the peak position in radians respectively. Thus, the average crystallite size is estimated to be ~19nm. Both crystallite size and microstrain (ε) can lead to peak broadening in the XRD spectrum. This value of microstrain can be determined from the W-H plot [10] (Figure 1B). The Williamson-Hall equation is given by:

$$\beta cos\theta = \frac{0.9\lambda}{D} + 4\varepsilon sin\theta \quad (2)$$

The values of D and ε can be determined by performing linear fit on the graph plotted between 4 sinθ and β cosθ where the slope of the line gives ε and D can be computed from the y-intercept. Thus, the estimated values of size and strain are ~21nm and 0.0005 respectively. The value of D agrees with the same measured using the Scherrer formula. The positive value of ε implies lattice elongation which is again verified using Nelson-Riley(N-R) plot (Figure 1C). In the N-R plot, f(θ)/2 is plotted against the lattice parameter calculated for different planes where the Nelson-Riley function, f(θ)[11] is given by:

$$f(\theta) = \left[\frac{cos^2\theta}{sin\theta} + \frac{cos^2\theta}{\theta}\right] \quad (3)$$

The value of the lattice parameter for which the N-R function becomes zero gives the corrected lattice parameter which is obtained as 10.64 Å. The increase in the value of the lattice parameter again confirms lattice elongation caused due to doping. The ionic radius of Eu^{3+} (1.07 Å) is slightly larger compared to that of Y^{3+}(1.01 Å)[12] and this can be the reason for the lattice elongation.

Figure 2A represents the UV-vis absorbance spectrum which indicates the material's absorption in the short UV region. The Tauc plot (Figure 2B) suggests that the material possesses a direct band gap energy of ~6eV. The

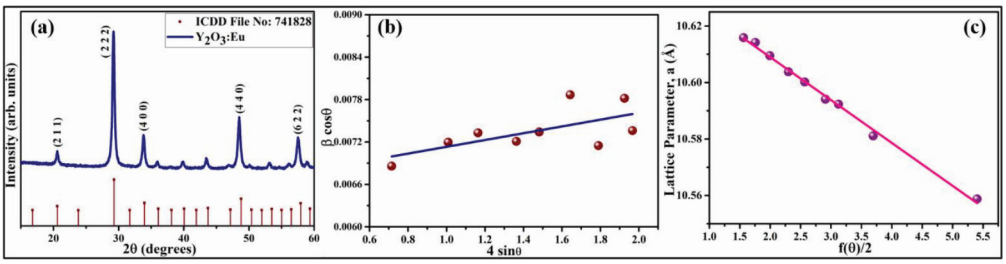


Figure 1. X-ray diffraction analysis**. (A)** XRD spectrum, **(B)** W-H plot for determination of lattice strain and **(C)** N-R plot measuring the corrected lattice parameter for Y_2O_3: Eu nanoparticles.

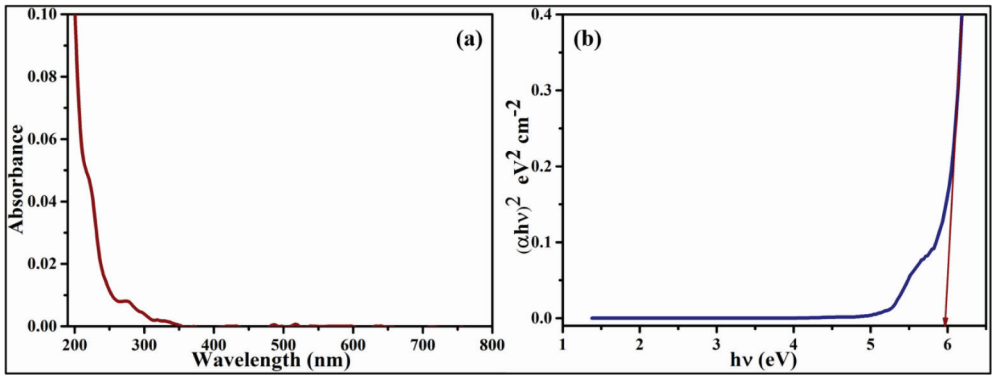


Figure 2. Bandgap estimation using UV-Vis Absorption spectroscopy. **(A)** Absorbance spectrum and **(B)** Tauc plot for the measurement of bandgap energy.

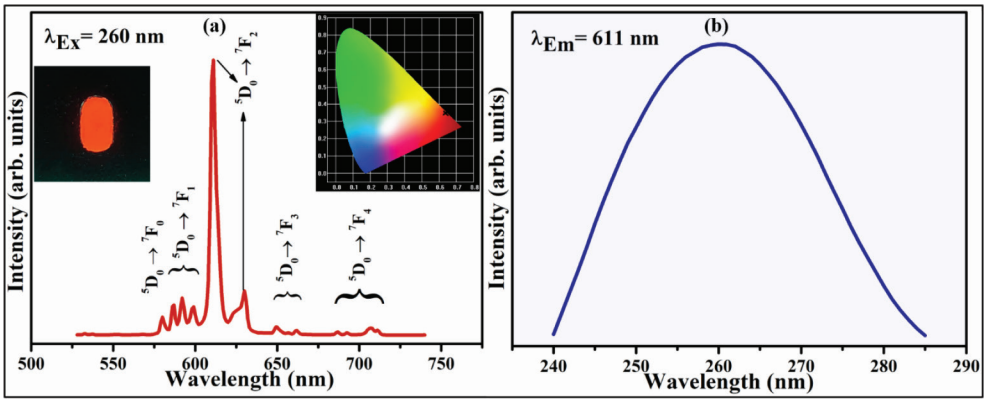


Figure 3. Photoluminescence Experiment confirming red emission. **(A)** Emission spectrum which shows different transitions between Eu^{3+} energy levels. Inset (Left) illustrates the intense red emission produced by the Y_2O_3: Eu nanoparticles and Inset (Right) shows the CIE chromaticity Diagram **(B)** PL Excitation spectrum.

size effect can be the reason for the increased band gap energy compared to bulk (~5.8eV).

The outcomes from the photoluminescence studies performed on the sample are presented in Figure 3. The PL emission spectrum (Figure 3A) shows that the material exhibits intense red emission centred at 611nm. The narrow emission lines can be recognised as the transitions from the excited state $^5D_0$ to the various ^7F_J (J=0,1,2,3,4) levels of Eu^{3+} ions[13,14]. The dominant line in the emission spectrum at 611 nm is identified as the $^5D_0 \rightarrow ^7F_2$ transition[15]. All transitions are marked in the spectrum. A photograph of intense red luminescence produced by the sample is shown in the inset of Figure 3A. To quantify the red colour, CIE coordinates are calculated and the (x, y) values are obtained as (0.64, 0.35). The CIE diagram is also shown in the inset of Figure 3A. The excitation spectrum shown in Figure 3B consists of a broad peak centred at 260nm. The emission spectrum was recorded at 260nm thus exciting the sample to a level above the bandgap energy.

4.0 Conclusions

Eu^{3+} doped Yttrium Oxide nano phosphor was successfully prepared using the wet chemical precipitation method followed by annealing at 600°C. The material possesses a cubic structure and exhibits lattice elongation which is confirmed by analysing the XRD results. The measured crystallite size falls in the nano regime. The precise value of the lattice parameter is determined using the Nelson-Riley plot. From PL experiments, intense red emission was observed under UV excitation thus proving the material's phosphor characteristics. Thus, the prepared Y_2O_3: Eu nanophosphor can have applications in the display industry. Hence, the prepared Y_2O_3: Eu nanophosphor

holds potential applications in the display industry, and its unique luminescent properties make it ideal for geologists to identify europium-doped oxides during the mining process.

5.0 Acknowledgment

SGN expresses gratitude to University Grants Commission (UGC) for the support received through JRF (UGC-Ref. No.: 1292/ (CSIR-UGCNET JUNE 2018)).

6.0 References

1. Cho SH, Kwon SH, Yoo JS, Oh CW, Lee JD, Hong KJ, *et al*. Cathodoluminescent characteristics of a spherical Y_2O_3: Eu phosphor screen for field emission display application. J Electrochem Soc. 2000; 147(8):3143. https://doi.org/10.1149/1.1393872
2. Kannan SK, Sundrarajan M. Biosynthesis of yttrium oxide nanoparticles using *Acalypha indica* leaf extract. Bull Mater Sci. 2015; 38(4):945-950. https://doi.org/10.1007/s12034-015-0927-7
3. Ianoș R, Băbuță R, Lazău R. Characteristics of Y_2O_3 powders prepared by solution combustion synthesis in the light of a new thermodynamic approach. Ceram Int. 2014; 40(8A):12207-12211. https://doi.org/10.1016/j.ceramint.2014.04.062
4. Popovici EJ, Muresan L, Amalia H, Indrea E, Vasilescu M. Synthesis and characterisation of europium activated yttrium oxide fine powders. J Alloys Compd. 2007; 434-435(SPEC. ISS.). https://doi.org/10.1016/j.jallcom.2006.08.312
5. J, Jagannathan R, Kutty TRN, Lu CH. Photoluminescence characteristics of Y_2O_3:Eu^{3+} nano phosphors prepared using sol-gel thermolysis. J Phys Chem B. 2001; 105(45):11098-11105. https://doi.org/10.1021/jp0119330
6. Muresan L, Popovici EJ, Imre-Lucaci F, Grecu R, Indrea E. Studies on Y_2O_3:Eu phosphor with different particle size prepared by wet chemical method. J Alloys Compd. 2009; 483(1-2). https://doi.org/10.1016/j.jallcom.2008.08.087
7. Muresan L, Popovici EJ, Grecu R, Tudoran LB. Studies on the synthesis of europium-activated yttrium oxide by wet-chemical method. 1. Influence of precursor quality on phosphor photoluminescence properties. J Alloys Compd. 2009; 471(1-2). https://doi.org/10.1016/j.jallcom.2008.03.100
8. Muresan L, Popovici EJ, Indrea E. Structural and luminescence characterization of yttrium oxide based phosphors prepared by wet- Chemical method. J Optoelectron Adv Mater. 2011; 13(3):183-189.
9. Safeera TA, Khanal R, Medvedeva JE, Martinez AI, Vinitha G, Anila EI. Low-temperature synthesis and characterization of zinc gallate quantum dots for optoelectronic applications. J Alloys Compd. 2018; 740:567-573. https://doi.org/10.1016/j.jallcom.2018.01.035
10. Mustapha S, Ndamitso MM, Abdulkareem AS, Tijani JO, Shuaib DT, Mohammed AK, *et al*. Comparative study of crystallite size using Williamson-Hall and Debye-Scherrer plots for ZnO nanoparticles. Adv Nat Sci Nanosci Nanotechnol. 2019; 10(4). https://doi.org/10.1088/2043-6254/ab52f7
11. Nelson JB, Riley DP. An experimental investigation of extrapolation methods in the derivation of accurate unit-cell dimensions of crystals. Proc Phys Soc. 1945; 57(3). https://doi.org/10.1088/0959-5309/57/3/302
12. Behrsing T, Deacon GB, Junk PC. The chemistry of rare earth metals, compounds, and corrosion inhibitors. In: Rare Earth-Based Corrosion Inhibitors. 2014. https://doi.org/10.1533/9780857093585.1
13. Thomas NM, Anila EI. Synthesis and characterisation of $SrAl_2O_4$: Eu^{3+} orange-red emitting nanoparticles. J Fluoresc. 2023; https://doi.org/10.1007/s10895-023-03351-8 PMid:37490253.
14. Bindu KR, Safeera TA, Anila EI. Pure red luminescence and concentration-dependent tunable emission color from europium-doped zinc sulfide nanoparticles. J Mater Sci Mater Electron. 2022; 33(22):17793-177801. https://doi.org/10.1007/s10854-022-08644-5
15. Binnemans K. Interpretation of europium(III) spectra. Coord Chem Rev. 2015; 295:1-45. https://doi.org/10.1016/j.ccr.2015.02.015